THE JOURNAL OF PHYSICAL CHEMISTRY A
A JOURNAL OF THE AMERICAN CHEMICAL SOCIETY

pubs.acs.org/JPCA Article

Benzene, Toluene, and Monosubstituted Derivatives: Diabatic Nature of the Oscillator Strengths of $S_1 \leftarrow S_0$ Transitions

David Robinson,* Saleh S. Alarfaji, and Jonathan D. Hirst

Cite This: https://doi.org/10.1021/acs.jpca.1c01685 Read Online

ACCESS | Metrics & More | Article Recommendations | Supporting Information

ABSTRACT: For benzene, toluene, aniline, fluorobenzene, and phenol, even sophisticated treatments of electron correlation, such as MRCI and XMS-CASPT2 calculations, show oscillator strengths typically lower than experiment. Inclusion of a simple pseudo-diabatization approach to perturb the S_1 state with approximate vibronic coupling to the S_2 state for each molecule results in more accurate oscillator strengths. Their absolute values agree better with experiment for all molecules except aniline. When the coupling between the S_1 and S_2 states is strong at the S_0 geometry, the simple diabatization scheme performs less well with respect to the oscillator strengths relative to the adiabatic values. However, we expect the scheme to be useful in many cases where the coupling is weak to moderate (where the maximum component of the coupling has a magnitude less than 1.5 au). Such calculations give an insight into the effects of vibronic coupling of excited states on UV/vis spectra.

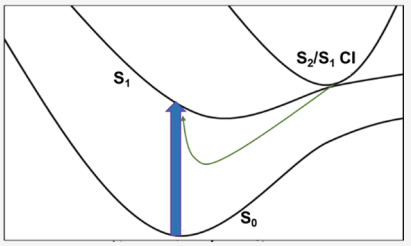

INTRODUCTION

Small monosubstituted benzenes serve as model systems for biological chromophores, helping to understand the structure of proteins[1] and hydrogels.[2] Both their electronically excited states[3] and their vibrational spectra have been widely investigated. For example, the aromatic groups of tyrosine and phenylalanine contribute to the electronic circular dichroism of proteins in the near ultraviolet,[4] while IR spectroscopy is widely used to probe the conformational landscape of proteins. Toluene plays a role in atmospheric chemistry, oxidizing in the troposphere and playing a role in secondary organic aerosol formation.[5−8] Toluene is also important for the synthesis of industrial polymers,[9] and excited states have a key role in the radiolysis of aromatic compounds.[10] A comprehensive description of the spectroscopy of individual chromophores is a pre-requisite for understanding the often complex spectra of dimers[11] and higher aggregates present in many types of macromolecular systems. We have a long-standing interest in the accurate and efficient description of the spectroscopy of toluene as a model of phenylalanine for electronic circular dichroism calculations. Such calculations determine parameters for our DichroCalc software.[12,13] In particular, we are interested in a simple, efficient, and quantitative approach to the calculation of vibronic coupling of different electronically excited states in such molecules to improve the fine structure of the electronic transitions and corresponding transition dipole moments.

To glean useful information from calculations of the electronic excited states of benzene and monosubstituted benzene derivatives, one must understand the nature of the transitions being studied: in our case, the $S_1 \leftarrow S_0$ transition. In benzene, the $S_1 \leftarrow S_0$ ($\tilde{A}^1B_{2u} \leftarrow \tilde{X}^1A_{1g}$) transition is formally forbidden, but it becomes allowed because of vibronic coupling to the optically allowed $\tilde{C}^1E_{1u}$ state.[14,15] Monosubstituted halobenzenes have C_{2v} symmetry, and so the $S_1 \leftarrow S_0$ transition becomes formally allowed, exhibiting a larger oscillator strength than benzene, although still weak. This is often stated as the electronic structure of monosubstituted benzenes having a "memory" of the D_{6h} symmetry and vibronic nature of the transition. Experimental studies have consistently shown some intensity, with activity in the b_2 vibrational modes in the $S_1 \leftarrow S_0$ spectra.[16] The S_2 state is known to have a conical intersection, leading to fast internal conversion to the S_1 state, with the S_2 state having a lifetime of less than 100 fs.[17,18] Once on the S_1 surface, the excitation wavepacket is able to decay along two channels: the first to the nearby S_1/S_0 conical intersection and the second to the S_1 minimum.[19] The S_1 state is longer lived, with a lifetime of ∼4 ps.[20]

There have been several different computational approaches to the accurate description of S_1 vibrational frequencies of aromatic molecules and vibronic coupling of S_1 states to higher electronic states for benzene, toluene, and other monosubstituted benzene derivatives. The vibronic bands in benzene have been investigated using multireference approaches,[21] and coupling between different states[22] has been considered in the interpretation of the photochemistry observed experimentally (see also ref 23 for a useful review by Suzuki). Tew et al. investigated the anharmonic nature of the S_1 vibrational

Received: February 24, 2021
Revised: May 5, 2021

frequencies of toluene using the CC2/cc-pVTZ approach.[24] They found several modes with substantial anharmonicity, and their overall agreement with experiment was within 30 cm^{-1} for all vibrational modes. Wang et al. studied the quantum dynamics of aniline, discovering vibronic coupling between the S_1 state and two Rydberg states.[25] Lykhin et al. also showed the importance of triplet states in the photodynamics of aniline, with a competitive photorelaxation route from the $^1\pi\pi^*$ state.[26] Mondal and Mahapatra determined that the S_1 state of fluorobenzene was coupled to a manifold of higher singlet excited states by constructing a vibronic Hamiltonian based on EOM-CCSD calculations.[27,28] Phenol exhibits vibronic coupling between the S_1 state and the dissociative S_2 state of a $\pi\sigma^*$ character.[29] Much theoretical work has been performed, confirming the nature of this conical intersection and tunneling, which is also part of the photodissociation pathway.[30−33] While each of these approaches shows good qualitative and quantitative accuracy in the low energy transitions for these molecules, they require specialist work and attention crafted for each individual molecule and are not applicable in an "off-the-shelf" sense, accessible to users from different disciplines.

In the current work, we investigate the $S_1 \leftarrow S_0$ transition in toluene. We employ a simple diabatization scheme to include vibronic coupling effects approximately. This scheme is applied to benzene and four monosubstituted derivatives to explore oscillator strength enhancement from vibronic coupling for multireference CI (MRCI) and XMS-CASPT2 calculations that is amenable to non-specialist users.

COMPUTATIONAL DETAILS

The S_0 and S_1 equilibrium geometries and S_2/S_1 minimum energy conical intersection (MECI) geometry for each of the molecules in Figure 1 were calculated at the XMS-CASPT2/cc-pVTZ level of theory (active spaces shown in Figure 1; in each case, the π-electron system plus lone pairs were included).

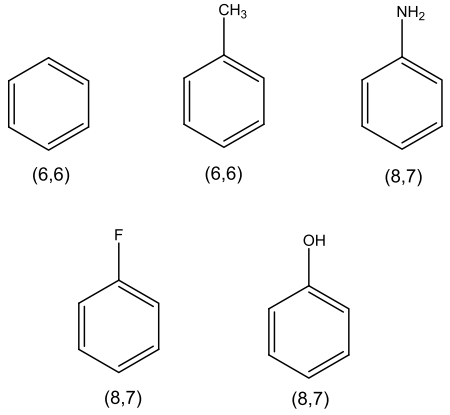

Figure 1. Benzene and the monosubstituted benzene derivatives investigated in this work. CASSCF active spaces are given in parentheses, where the notation is (number of active electrons, number of active orbitals).

Vibronic coupling is a process where the Born−Oppenheimer approximation breaks down and an adiabatic electronic state, J, mixes with another adiabatic electronic state, I, due to vibrations of the nuclei:

$$f_{JI}(\boldsymbol{R}) = \langle \Psi_J(\boldsymbol{R}) | \frac{\partial}{\partial q} | \Psi_I(\boldsymbol{R}) \rangle \tag{1}$$

where f_{JI} are the non-adiabatic coupling matrix elements (NACMEs) and $\boldsymbol{R}$ are the nuclear coordinates. The effects of vibronic coupling were included using the simple diabatization scheme of Simah et al.[34] (based on the work by Domcke and Woywod[35]), in which the overlap of the orbitals from a reference geometry and target geometry is optimized and the resulting pseudo-diabatic orbitals are used to transform the wavefunction at the target geometry. In our case, we chose the reference geometry to be the MECI of the S_2/S_1 conical intersection seam, as this is the point at which the two states involved in the intensity borrowing process interact most strongly. The target geometry is the S_0 optimized geometry as this represents the geometry at which the Franck−Condon (FC) excitation occurs. The diabatic states (denoted by the superscript d) are considered to be a minor perturbation to the adiabatic states and are found by a unitary transformation of the S_1 and S_2 adiabatic states (denoted by a superscript a)

$$\Psi^d_m = \sum_n \Psi^a_n U_{nm} \tag{2}$$

The unitary transformation matrix is chosen such that the NACME vector, X_2

$$X_2 = \langle \Psi^d_m | \frac{\partial}{\partial q} | \Psi^d_n \rangle \tag{3}$$

is minimized for all of the internal coordinates, q. For a two-state diabatization, the unitary transformation matrix, $\mathbf{U}$, is given as

$$\mathbf{U} = \begin{bmatrix} \cos\theta & \sin\theta \\ -\sin\theta & \cos\theta \end{bmatrix} \tag{4}$$

where a single non-adiabatic mixing angle, θ, can be used to describe the mixing of the adiabatic states. In the approximate scheme used in this work, the CI coefficients from an MRCI or XMS-CASPT2 calculation were transformed by maximizing the overlap of the CASSCF orbitals at the S_0 geometry with those obtained at a reference geometry, generating a pseudo-diabatic set of orbitals:

$$|\langle \phi_i(q') | \phi_i(q) \rangle|^2 + |\langle \phi_j(q') | \phi_j(q) \rangle|^2 \tag{5}$$

where the overlap is computed over all active orbitals i and j at the current geometry q with those at the reference geometry q', which in this case was the S_2/S_1 MECI. In all cases, we assume that this MECI lies close to the S_1 minimum and the proximity of the electronic states allows them to interact (see Figure 2 for a qualitative overview). The diabatic wavefunction, Ψ^d_m, is constructed from the pseudo-diabatic orbitals as

$$\Psi^d_m = \sum_I^N d_{Im} \Phi^d_I \tag{6}$$

At the target geometry, the matrix $\mathbf{d}$ is related to the adiabatic wavefunctions by the transformation $\mathbf{d} = \mathbf{cU}$, where $\mathbf{c}$ is the coefficient matrix of the adiabatic wavefunctions and $\mathbf{U}$ is determined using the condition that $\mathbf{d}$ remains as close as possible to the matrix $\mathbf{d}^{ref}$ at the reference geometry:

$$\mathbf{U} = \mathbf{V}(\mathbf{V}^\dagger \mathbf{V})^{-1/2} \tag{7}$$

where

https://doi.org/10.1021/acs.jpca.1c01685
J. Phys. Chem. A XXXX, XXX, XXX−XXX

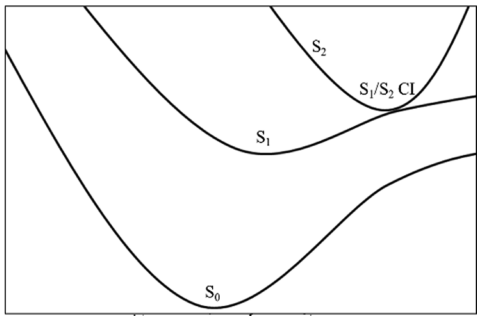

Figure 2. Qualitative schematic of the S_0, S_1, and S_2 potential energy surfaces in the region of the Franck−Condon excitation.

$$\mathbf{V} = \mathbf{c}^{\dagger}\mathbf{d}^{\mathrm{ref}} \tag{8}$$

The transition dipole moments can then be calculated for the $S_1 \leftarrow S_0$ transition, with the approximately diabatic S_1 state, as

$$\overrightarrow{\mu_x} = \langle \Psi^d_{S_1} | \mu_x | \Psi^a_{S_0} \rangle \tag{9}$$

and similarly for the $\overrightarrow{\mu}_y$ and $\overrightarrow{\mu}_z$ components using either the MRCI or XMS-CASPT2 computed densities. Writing the energy expressions explicitly for each of the two states, one obtains

$$E^d_{S_1} = (\cos^2\theta)E^a_{S_1} + (\sin^2\theta)E^a_{S_2} \tag{10a}$$

$$E^d_{S_2} = (\sin^2\theta)E^a_{S_1} + (\cos^2\theta)E^a_{S_2} \tag{10b}$$

The oscillator strength can then be calculated:

$$f = \frac{2}{3}(E^d_{S_1} - E^a_{S_0})|\langle \Psi^d_{S_1} | \mu | \Psi^a_{S_0} \rangle|^2 \tag{11}$$

While in eq 11, we use an adiabatic description of the S_0 state and pseudo-diabatic representation for S_1, the pseudo-diabatic representation is essentially only a perturbation to the adiabatic S_1 state. As such, where there is very strong coupling between S_1 and S_2 states, we expect this simple approximation to break down as the pseudo-diabatization scheme is based on the assumption that the orbitals and CI coefficients change very little as a function of geometry; this is not always true in the vicinity of a conical intersection. In the original scheme of Simah et al.,[34] the reference geometry is ideally chosen where the adiabatic and diabatic states are identical (e.g., due to symmetry). In the current work, the use of the S_2/S_1 MECI is a point at which the NACME terms do not vanish completely, but the adiabatic and diabatic states may not be identical. Additionally, the reference orbitals at the MECI geometry may have poor overlap with those at the target geometry (S_0). If the MECI is far from the FC region of the S_1 state, then the current scheme is likely to show limited vibronic coupling, even if there is true coupling between the two states.

Adiabatic XMS-CASPT2[36] calculations were performed within the single-state single-reference contraction scheme (SS-SR) and a real shift of 0.2 au, using the cc-pVTZ basis[37] and the cc-pVTZ-JKFIT auxiliary basis set,[38] using the BAGEL software.[39,40] Adiabatic time-dependent density functional theory (TDDFT) calculations within the Tamm−Dancoff approximation[41] were performed with the B3LYP,[42] CAM-B3LYP,[43] M06-2X,[44] and ωB97X[45] functionals. Single-reference EOM-CCSD,[46] ADC(2),[47] and ADC(3)[48] calculations were also performed. TDDFT and single-reference wavefunction theory calculations were performed using the Q-Chem software.[49] The diabatic transformation calculations (using both internally contracted MRCI[50−52] and XMS-CASPT2) were performed with the Molpro software suite.[53] The S_0 and S_2/S_1 calculated geometries were superposed based on minimizing the RSMD of all atoms. In all cases, the cc-pVTZ basis set[37] was employed as it represents a good compromise between accuracy and computational cost.

In addition, for toluene, a vibrationally resolved spectrum was determined by calculating the FC factors between the S_0 and S_1 harmonic vibrational modes and frequencies. The spectrum was calculated using the ezSpectrum software[54,55] at a temperature of 10 K.

RESULTS AND DISCUSSION

We first consider the S_0 and S_1 states of toluene. In Table 1 are the calculated XMS-CASPT2 harmonic vibrational frequencies.

Table 1. Calculated Harmonic Frequencies of the S_0 and S_1 States of Toluene (XMS-CASPT2/cc-pVTZ)[c]

	S_0		S_1	
assignment[a]	XMS-CASPT2	Expt.[b]	XMS-CASPT2	Expt.[b]
m_1	3072	3087	3086	3097
m_2	3052	3063	3076	3077
m_3	3038	3055	3066	3063
m_4	1560	1605	1411	
m_5	1439	1494	1401	
m_6	1179	1210	1162	1193
m_7	1136	1175	1110	1021
m_8	1003	1030	921	935; 934
m_9	949	1003	904	966
m_{10}	751	785	719	736; 753
m_{11}	492	521	435	457
m_{12}	798	964	514	687
m_{13}	751	843	511	
m_{14}	379	407	211	228; 226
m_{15}	798	978	583	
m_{16}	751	895	514	697
m_{17}	637	728	511	
m_{18}	379	695	309	423
m_{19}	317	464	287	320; 314
m_{20}	197	216	131	157; 145
m_{21}	3058	3039	3086	3087
m_{22}	3038	3029	3066	3048
m_{23}	1560	1586	1528	
m_{24}	1424	1445	1411	
m_{25}	1340	1312	1331	
m_{26}	1277	1280	1248	
m_{27}	1136	1155	1110	
m_{28}	1049	1080	1000	
m_{29}	587	623	514	532
m_{30}	317	342	309	332; 331

[a]Assignments taken from ref 14. [b]Experimental data taken from refs 16, 56, 58. [c]Harmonic frequencies are scaled by 0.954. See the Supporting Information for full details of the scaling parameter.

The scaled harmonic vibrational frequencies show fair agreement with experiment,[16,56−58] with a maximum error of 316 cm^{-1} for one of the low frequency carbon−carbon bend modes (m_{18}) and average errors of 55 and 29 cm^{-1} for the S_0 and S_1 frequencies, respectively, after scaling. The average error for the S_0 vibrations is 45 cm^{-1}, neglecting the m_{18} frequency. Tew et al. employed the CC2/cc-pVTZ approach to calculate

https://doi.org/10.1021/acs.jpca.1c01685
J. Phys. Chem. A XXXX, XXX, XXX−XXX

anharmonic frequencies of toluene.[24] The differences exhibited between the XMS-CASPT2 and experimental S_1 frequencies are likely due to a combination of anharmonicity, for which CC2/cc-pVTZ performs well,[24] and potential issues in the XMS-CASPT2 accuracy. In particular, the m_4, m_{12}, m_{15}, m_{16}, m_{18}, m_{23}, and m_{25} modes all show larger differences to the CC2 values (and experiment); these were modes identified as genuinely anharmonic.[24] Battaglia and Lindh determined XMS-CASPT2 excitations to be poor relative to MS-CASPT2 in regions where potential surfaces are energetically well separated (i.e., at or near minima); they developed an alternative approach to XMS-CASPT2 termed extended dynamically weighted CASPT2 (XDW-CASPT2).[59] The results presented here suggest that stationary points and their frequencies may be similarly affected. These frequencies have been used to generate a vibrationally resolved spectrum (Figure 3). The dominant transition is the 0−0 vibrational line, with a handful of other vibrational lines about two orders of magnitude smaller.

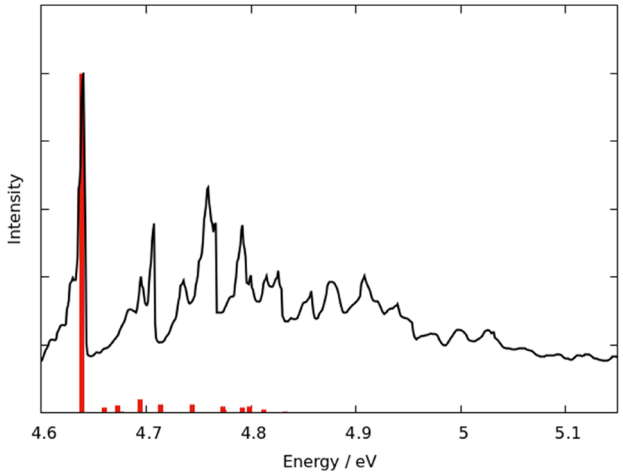

Figure 3. Experimental (line) and computed (stick) spectrum of the $S_1 \leftarrow S_0$ transition for toluene. The computed spectrum has been shifted by −0.136 eV to match the experimental spectrum.[60]

We now turn to the calculation of the oscillator strengths for the $S_1 \leftarrow S_0$ transition for toluene, benzene, and three monosubstituted benzene derivatives. The S_2/S_1 MECI structures for each of the molecules considered are shown in Figure 4. With the exception of aniline, all exhibit a prefulvene-like structure typical of the MECI geometries of aromatic molecules. Aniline exhibits geometrical distortion of the $-NH_2$ group relative to the ring, with the atoms in the ring remaining planar. This is similar to that seen for the $^1\pi\pi^*/^1\pi\sigma^*$ MECI in the recent work of Ray and Ramesh.[61] The MECI geometry for toluene has a peaked topology, while the rest have a sloped topology.

The computed transition energies are given in Table 2 (0−0 transitions) and Table 3 (Franck−Condon transitions), along with the calculated oscillator strengths. The MECIs lie 1.14, 0.89, 0.52, 0.59, and 1.10 eV above the S_1 minima and 0.97, 0.73, 0.28, 0.42, and 1.03 eV above the Franck−Condon transition energy ($S_1 \leftarrow S_0$) for benzene, toluene, aniline, fluorobenzene, and phenol, respectively. The magnitudes of the calculated and experimental oscillator strengths[62] are compared in Figure 5. The single-reference methods generally overestimate the oscillator strength, although for benzene (data shown in Table 3) and toluene, they are between 0 and 50% of the experimental value. The multireference methods both underestimate the oscillator strengths in comparison to experiment and the single-reference methods (DFT, EOM-CCSD, and ADC approaches), with the exception of phenol, where the XMS-CASPT2 oscillator strength is the largest of all the methods considered. The pseudo-diabatic oscillator strengths are given in Table 3 and Figure 5 for MRCI and XMS-CASPT2. The calculated oscillator strengths are enhanced relative to the adiabatic values for all molecules except aniline, where the pseudo-diabatic values are ∼50% of the adiabatic values and ∼10% of the experimental value for both MRCI and XMS-CASPT2. In this case, we can see that the S_2 state is energetically close to the S_1 state across the potential energy surface connecting the S_0 minimum and S_2/S_1 conical intersection (see Figure S1), deviating by no more than ∼1.1 eV. In contrast, the other molecules have energy gaps

Table 2. Calculated Energy Differences (XMS-CASPT2/cc-pVTZ) between the Minima for the S_0 and S_1 States of Each Molecule and Their S_2S_1 MECIs

molecule	ΔE (0−0, $S_1 \leftarrow S_0$) (eV)	ΔE ($S_2/S_1 \leftarrow S_0$) (eV)
benzene	4.72	5.86
toluene	4.60	5.49
aniline	4.29	4.81
fluorobenzene	4.69	5.28
phenol	4.53	5.63

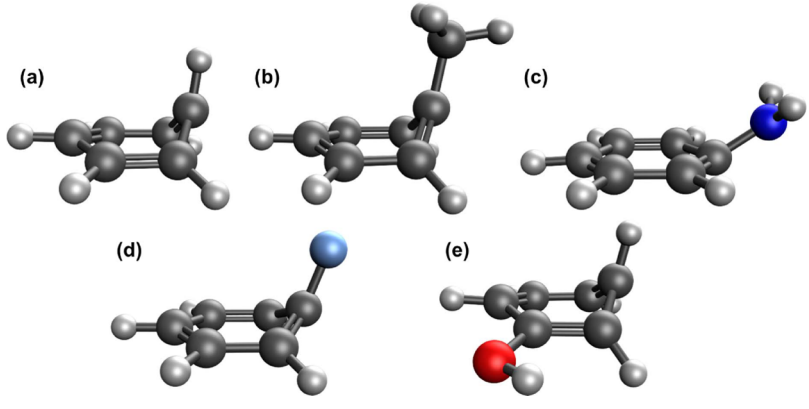

Figure 4. XMS-CASPT2/cc-pVTZ structures for the S_2/S_1 MECI of (a) benzene, (b) toluene, (c) aniline, (d) fluorobenzene, and (e) phenol.

https://doi.org/10.1021/acs.jpca.1c01685
J. Phys. Chem. A XXXX, XXX, XXX−XXX

Table 3. Computed Franck−Condon Excitation Energies (in eV) and Oscillator Strengths in the Adiabatic and Pseudo-diabatic Basis[a]

	benzene		toluene		aniline		fluorobenzene		phenol	
method	ΔE	f	ΔE	f	ΔE	f	ΔE	f	ΔE	f
Adiabatic										
MRCI	5.08	0.0000	4.98	0.0000	4.83	0.0074	5.08	0.0025	4.96	0.0070
XMS-CASPT2	4.89	0.0000	4.76	0.0001	4.53	0.0080	4.86	0.0025	4.59	0.0531
EOM-CCSD	5.18	0.0000	5.12	0.0011	4.78	0.0384	5.24	0.0097	5.07	0.0234
ADC(2)	5.25	0.0000	5.16	0.0013	4.71	0.0464	5.26	0.0152	5.04	0.0323
ADC(3)	4.98	0.0000	4.91	0.0013	4.59	0.0389	5.05	0.0092	4.89	0.0227
B3LYP	5.50	0.0000	5.31	0.0017	4.80	0.0501	5.43	0.0133	5.20	0.0330
CAM-B3LYP	5.66	0.0000	5.43	0.0021	5.04	0.0561	5.60	0.0147	5.39	0.0359
M06-2X	5.71	0.0000	5.51	0.0021	5.10	0.0573	5.67	0.0153	5.47	0.0361
ωB97X	5.69	0.0000	5.49	0.0022	5.12	0.0576	5.63	0.0155	5.44	0.0369
Diabatic										
MRCI	5.05	0.0029	5.47	0.0066	4.84	0.0033	5.45	0.0042	5.01	0.0080
XMS-CASPT2	4.91	0.0048	5.21	0.0097	4.80	0.0044	5.38	0.0074	4.99	0.0118
Expt.	4.88	0.0006	4.62	0.0050	3.69	0.0355	4.73	0.0076	4.56	0.0161

[a]Experimental data taken from ref 62.

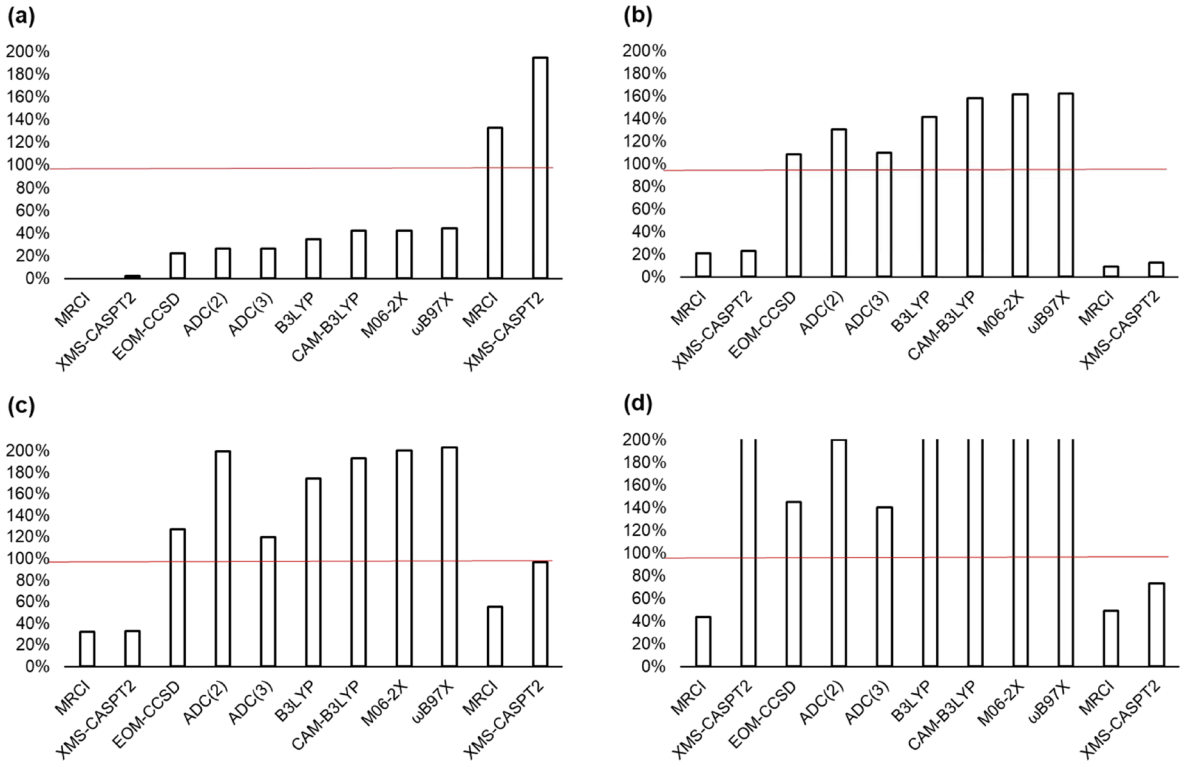

Figure 5. Calculated oscillator strengths expressed as a percentage of the experimental value. A value of 100% corresponds to the experimental value. The final two columns of each plot are the pseudo-diabatic MRCI and XMS-CASPT2 oscillator strengths. (a) Toluene; (b) aniline; (c) fluorobenzene; and (d) phenol. Values greater than 200% are depicted with open boxes.

greater than 1.5 eV at the S_0 minima. In Figure 6, we present visual representations of the XMS-CASPT2 calculated non-adiabatic coupling vector between the S_2 and S_1 states at the S_0 geometry. It is clear for aniline that the coupling is much stronger than that seen for the other molecules. This is also reflected in the Franck−Condon excitation energy being less than 0.3 eV lower than the S_2/S_1 MECI relative to the S_0 energy. Interestingly, the coupling is strongest for the atoms in the ring and relatively low for the $-NH_2$ group, in contrast to the $^1\pi\pi^*/^1\pi\sigma^*$ conical intersection.[61] Worth and co-workers demonstrated two 3p Rydberg states between the S_1 and S_2 states. These also couple to the S_1 state,[25] but they are not considered in the current study. We propose that, in this case, the approximate diabatization scheme would need to be replaced with a more robust approach (possibly including Franck−Condon factors and explicit integration of the NACMEs) to give a more accurate oscillator strength as vibronic coupling between the S_1 and S_2 states is stronger than the other molecules considered. Given in Figure S2 are the maximum and average coupling values compared to the difference in oscillator strength between the calculated and experimental oscillator strengths. For the molecules consid-

https://doi.org/10.1021/acs.jpca.1c01685
J. Phys. Chem. A XXXX, XXX, XXX−XXX

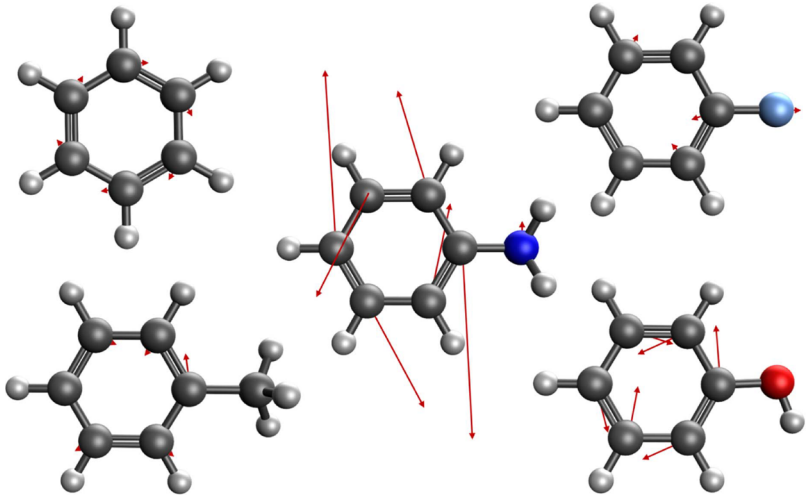

Figure 6. Visual representation of the non-adiabatic coupling vectors between the S_2 and S_1 states at the S_0 optimized geometries for benzene (top left), toluene (bottom left), aniline (center), fluorobenzene (top right), and phenol (bottom right).

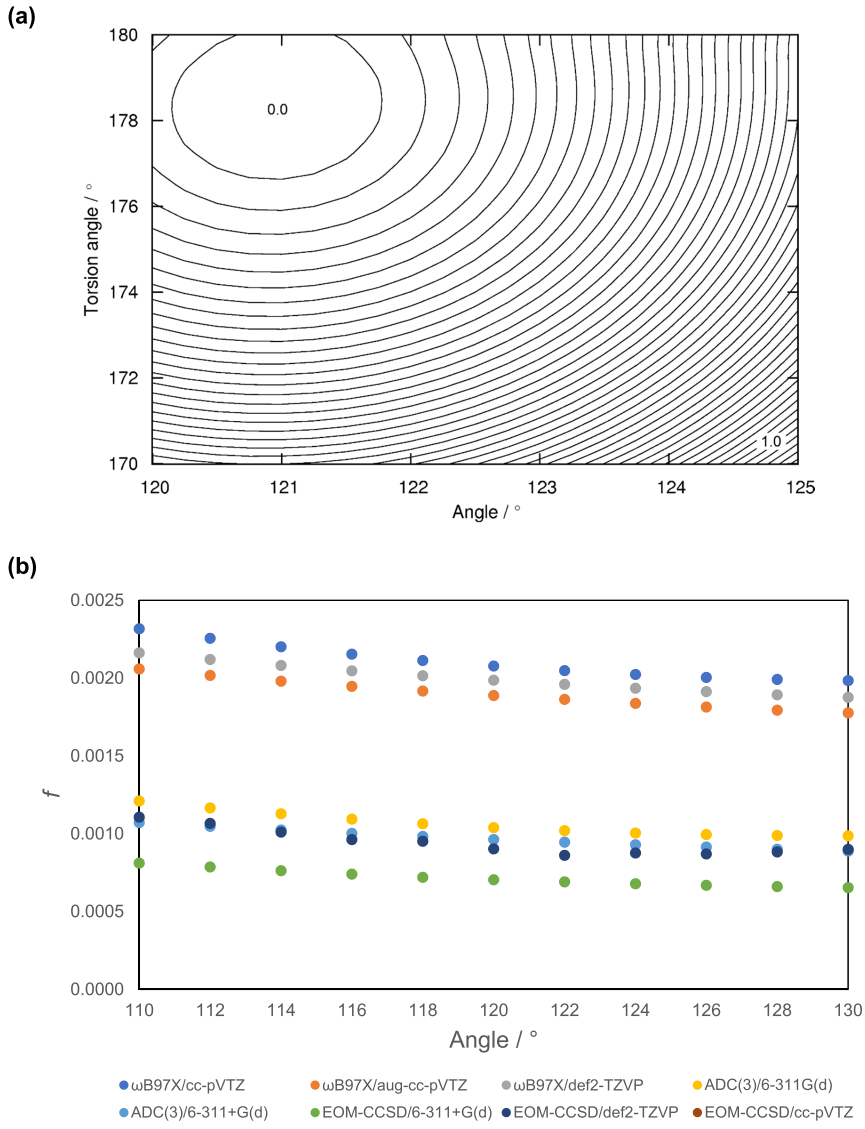

Figure 7. (a) Two-dimensional potential energy surface scanned along the torsion angle C(aromatic)−C(aromatic)−C(aromatic)−C(methyl) and the bond angle C(aromatic)−C(aromatic)−C(methyl); kcal mol^{-1}, contour value of 0.025 kcal mol^{-1}. (b) Calculated oscillator strength as a function of the bond angle C(aromatic)−C(aromatic)−C(methyl) (see key for details of the methods).

https://doi.org/10.1021/acs.jpca.1c01685
J. Phys. Chem. A XXXX, XXX, XXX−XXX

ered, the accuracy of the current method deteriorates when an individual atom's NACME vector has a magnitude greater than 1.5 au (or the average magnitude of the NACME vector across all atoms is greater than ∼0.7 au). The coupling between electronically excited states for phenol in this study is between two $^1\pi\pi^*$ states, while the true S_2 state is of a $\pi\sigma^*$ character.[63] This is a consequence of the approach taken in this study, namely, choosing the simple π-electron active space and not expanding to include σ^* orbitals.

For each of the molecules considered, the point-group symmetry of the geometry of the S_0 state is D_{6h} (benzene), C_s (toluene), C_{2v} (aniline), C_{2v} (fluorobenzene), and C_s (phenol). Breaking of the planar aromatic ring would therefore be assumed to be responsible for an enhancement in the oscillator strength of the $S_1 \leftarrow S_0$ transition. The effect of symmetry breaking upon the calculated oscillator strength is given in Figure 7 for toluene. As the torsion angle (between three aromatic carbon atoms and the methyl carbon) is decreased by ∼10°, the energy of the S_0 state increases by only 1 kcal mol^{-1} (Figure 7a). As such, there is effectively little to no barrier to symmetry breaking at finite temperature. While there is a small change in the oscillator strength as the symmetry of the molecule is broken, this is a small effect (Figure 7b).

We now consider the extent to which the S_1 and S_2 states are mixed in the pseudo-diabatization procedure. In Table 4 are

Table 4. Diabatic Rotation Angles Determined Using the Pseudo-diabatization Procedure[a]

molecule	θ (MRCI)	θ (XMS-CASPT2)
benzene	0.02	−0.01
toluene	−24.6	−20.6
aniline	0.1	0.1
fluorobenzene	−20.8	−21.8
phenol	8.7	11.1

[a]All angles in °.

the calculated diabatic rotation angles for MRCI and XMS-CASPT2 for each of the molecules considered. While these rotation angles have an effect on the diabatic energies (eq 7), the effect on the oscillator strengths is determined by the mixing of the CI coefficients. As noted above, the coupling between the S_2 and S_1 states is strong for aniline with analytic NACMEs at the S_0 geometry, in contradiction to the rotation angle calculated using the approximate pseudo-diabatization procedure. This provides further evidence that, in the event of strong coupling, the pseudo-diabatization procedure becomes less reliable.

CONCLUSIONS

We have applied a simple pseudo-diabatization scheme to benzene, toluene, and three other monosubstituted benzenes to account for the vibronic coupling between the S_2 and S_1 states and the effect this has upon the transition properties of the $S_1 \leftarrow S_0$ excitation using multireference approaches. In the adiabatic basis, MRCI and XMS-CASPT2 exhibit oscillator strengths lower than the experimental value. Inclusion of approximate vibronic coupling effects through the pseudo-diabatic states results in improved quantitative values of the oscillator strength for all molecules except aniline. In this case, the vibronic coupling was determined to be strong relative to that seen in the other molecules; the success of the simple approach adopted here is predicated on weak coupling of the S_2 and S_1 states; in the case of aniline, this coupling is strong, leading to a poor description of the oscillator strength.

ASSOCIATED CONTENT

Supporting Information

The Supporting Information is available free of charge at https://pubs.acs.org/doi/10.1021/acs.jpca.1c01685.

Potential energy scans for aniline, NACME magnitudes, and harmonic vibrational frequency scaling data (PDF)

AUTHOR INFORMATION

Corresponding Author

David Robinson − *Department of Chemistry and Forensics, School of Science and Technology, Nottingham Trent University, Nottingham NG11 8NS, United Kingdom;* orcid.org/0000-0003-2760-7163; Email: david.robinson@ntu.ac.uk

Authors

Saleh S. Alarfaji − *School of Chemistry, University of Nottingham, Nottingham NG7 2RD, United Kingdom;* Present Address: Present address: Research Center for Advanced Materials Science (RCAMS), King Khalid University, P. O. Box 9004, Abha, Saudi Arabia (S.S.A.).

Jonathan D. Hirst − *School of Chemistry, University of Nottingham, Nottingham NG7 2RD, United Kingdom;* orcid.org/0000-0002-2726-0983

Complete contact information is available at: https://pubs.acs.org/10.1021/acs.jpca.1c01685

Notes

The authors declare no competing financial interest.

ACKNOWLEDGMENTS

We thank NTU and the University of Nottingham (UoN) for provision of high performance computing facilities used for the present calculations. We thank Zhuo Li (UoN) for useful discussions. S.S.A. thanks the Research Center of Advanced Materials, King Khalid University in Saudi Arabia for a studentship (grant no. RCAMS/KKU/0020/20). J.D.H. is supported by the Royal Academy of Engineering under the Chairs in Emerging Technologies scheme.

REFERENCES

(1) Burley, S. K.; Petsko, G. A. Aromatic-Aromatic Interaction: A Mechanism of Protein Structure Stabilization. *Science* **1985**, *229*, 23−28.

(2) Li, J.; Du, X.; Hashim, S.; Shy, A.; Xu, B. Aromatic-Aromatic Interactions Enable α-Helix to β-Sheet Transition of Peptides to Form Supramolecular Hydrogels. *J. Am. Chem. Soc.* **2017**, *139*, 71−74.

(3) Pratt, D. W. High Resolution Spectroscopy in the Gas Phase: Even Large Molecules Have Well-Defined Shapes. *Annu. Rev. Phys. Chem.* **1998**, *49*, 481−530.

(4) Rogers, D. M.; Hirst, J. D. First-Principles Calculations of Protein Circular Dichroism in the near Ultraviolet. *Biochemistry* **2004**, *43*, 11092−11102.

(5) Finlayson-Pitts, B. J.; Pitts, J. N. *Chemistry of the Upper and Lower Atmosphere*; Elsevier, 1999.

(6) Calvert, J. G.; Atkinson, R.; Becker, K. H.; Kamens, R. M.; Seinfeld, J. H.; Wallington, T. J.; Yarwood, G. *The Mechanisms of Atmospheric Oxidation of the Aromatic Hydrocarbons*; Oxford University Press, 2002.

(7) Steinfeld, J. H.; Pandis, S. N. Atmospheric Chemistry and Physics: From Air Pollution to Climate Change. *Phys. Today* **1998**, *51*, 88−90.
(8) Ji, Y.; Zhao, J.; Terazono, H.; Misawa, K.; Levitt, N. P.; Li, Y.; Lin, Y.; Peng, J.; Wang, Y.; Duan, L.; et al. Reassessing the Atmospheric Oxidation Mechanism of Toluene. *Proc. Natl. Acad. Sci. U. S. A.* **2017**, *114*, 8169−8174.
(9) Schulze, M. Industrial Organic Chemicals. Von H. A. Wittcoff, B. G. Reuben, J. S. Plotkin. *Chem. Ing. Tech.* **2014**, *86*, 1304−1304.
(10) Baidak, A.; Badali, M.; Laverne, J. A. Role of the Low-Energy Excited States in the Radiolysis of Aromatic Liquids. *J. Phys. Chem. A* **2011**, *115*, 7418−7427.
(11) Rogers, D. M.; Hirst, J. D.; Lee, E. P. F.; Wright, T. G. Ab Initio Study of the Toluene Dimer. *Chem. Phys. Lett.* **2006**, *427*, 410−413.
(12) Jasim, S. B.; Li, Z.; Guest, E. E.; Hirst, J. D. DichroCalc: Improvements in Computing Protein Circular Dichroism Spectroscopy in the Near-Ultraviolet. *J. Mol. Biol.* **2018**, *430*, 2196−2202.
(13) Bulheller, B. M.; Hirst, J. D. DichroCalc—Circular and Linear Dichroism Online. *Bioinformatics* **2009**, *25*, 539−540.
(14) Gardner, A. M.; Wright, T. G. Consistent Assignment of the Vibrations of Monosubstituted Benzenes. *J. Chem. Phys.* **2011**, *135*, 114305.
(15) Douglas, I. N.; Grinter, R.; Thomson, A. J. Vibronic Borrowing of Angular Momentum in The $^1B_{2u}$ State of Benzene. *Mol. Phys.* **1975**, *29*, 673−679.
(16) Gardner, A. M.; Green, A. M.; Tamé-Reyes, V. M.; Wilton, V. H. K.; Wright, T. G. Vibrations of the Low Energy States of Toluene ($\tilde{X}\ ^1A_1$ and $\tilde{A}\ ^1B_2$) and the Toluene Cation ($\tilde{X}\ ^2B_1$). *J. Chem. Phys.* **2013**, *138*, No. 134303.
(17) Suzuki, Y.-I.; Horio, T.; Fuji, T.; Suzuki, T. Time-Resolved Photoelectron Imaging of S2 → S1 Internal Conversion in Benzene and Toluene. *J. Chem. Phys.* **2011**, *134*, No. 184313.
(18) Radloff, W.; Stert, V.; Freudenberg, T.; Hertel, I. V.; Jouvet, C.; Dedonder-Lardeux, C.; Solgadi, D. Internal Conversion in Highly Excited Benzene and Benzene Dimer: Femtosecond Time-Resolved Photoelectron Spectroscopy. *Chem. Phys. Lett.* **1997**, *281*, 20−26.
(19) Adachi, S.; Suzuki, T. Methyl Substitution Effects on the Non-Adiabatic Dynamics of Benzene: Lifting Three-State Quasi-Degeneracy at Conical Intersections. *Phys. Chem. Chem. Phys.* **2020**, *22*, 2814−2818.
(20) Farmanara, P.; Stert, V.; Radloff, W.; Hertel, I. V. Ultrafast Internal Conversion in Highly Excited Toluene Monomers and Dimers. *J. Phys. Chem. A* **2001**, *105*, 5613−5617.
(21) Bernhardsson, A.; Forsberg, N.; Malmqvist, P. Å.; Roos, B. O.; Serrano-Andrés, L. A Theoretical Study of the $^1B_{2u}$ and $^1B_{1u}$ Vibronic Bands in Benzene. *J. Chem. Phys.* **2000**, *112*, 2798−2809.
(22) Worth, G. A. A Model Hamiltonian to Simulate the Complex Photochemistry of Benzene. *J. Photochem. Photobiol., A* **2007**, *190*, 190−199.
(23) Suzuki, T. Time-Resolved Photoelectron Spectroscopy of Non-Adiabatic Electronic Dynamics in Gas and Liquid Phases. *Int. Rev. Phys. Chem.* **2012**, *31*, 265−318.
(24) Tew, D. P.; Hättig, C.; Graf, N. K. Anharmonic Excited State Frequencies of *para*-Difluorobenzene, Toluene and Catechol Using Analytic RI-CC2 Second Derivatives. *Phys. Chem. Chem. Phys.* **2019**, *21*, 14063−14072.
(25) Wang, F.; Neville, S. P.; Wang, R.; Worth, G. A. Quantum Dynamics Study of Photoexcited Aniline. *J. Phys. Chem. A* **2013**, *117*, 7298−7307.
(26) Lykhin, A. O.; Truhlar, D. G.; Gagliardi, L. Role of Triplet States in the Photodynamics of Aniline. *J. Am. Chem. Soc.* **2021**, *143*, 5878−5889.
(27) Mondal, T.; Mahapatra, S. Photophysics of Fluorinated Benzene. I. Quantum Chemistry. *J. Chem. Phys.* **2010**, *133*, No. 084304.
(28) Mondal, T.; Mahapatra, S. Photophysics of Fluorinated Benzene. II. Quantum Dynamics. *J. Chem. Phys.* **2010**, *133*, No. 084305.
(29) Lai, H. Y.; Jhang, W. R.; Tseng, C.-M. Communication: Mode-Dependent Excited-State Lifetime of Phenol under the S_1/S_2 Conical Intersection. *J. Chem. Phys.* **2018**, *149*, No. 031104.
(30) Vieuxmaire, O. P. J.; Lan, Z.; Sobolewski, A. L.; Domcke, W. Ab Initio Characterization of the Conical Intersections Involved in the Photochemistry of Phenol. *J. Chem. Phys.* **2008**, *129*, No. 224307.
(31) Xu, X.; Zheng, J.; Yang, K. R.; Truhlar, D. G. Photodissociation Dynamics of Phenol: Multistate Trajectory Simulations Including Tunneling. *J. Am. Chem. Soc.* **2014**, *136*, 16378−16386.
(32) Yang, K. R.; Xu, X.; Zheng, J.; Truhlar, D. G. Full-Dimensional Potentials and State Couplings and Multidimensional Tunneling Calculations for the Photodissociation of Phenol. *Chem. Sci.* **2014**, *5*, 4661−4680.
(33) Xie, C.; Ma, J.; Zhu, X.; Yarkony, D. R.; Xie, D.; Guo, H. Nonadiabatic Tunneling in Photodissociation of Phenol. *J. Am. Chem. Soc.* **2016**, *138*, 7828−7831.
(34) Simah, D.; Hartke, B.; Werner, H.-J. Photodissociation Dynamics of H_2S on New Coupled *Ab Initio* Potential Energy Surfaces. *J. Chem. Phys.* **1999**, *111*, 4523−4534.
(35) Domcke, W.; Woywod, C. Direct Construction of Diabatic States in the CASSCF Approach. Application to the Conical Intersection of the 1A2 and 1B1 Excited States of Ozone. *Chem. Phys. Lett.* **1993**, *216*, 362−368.
(36) Shiozaki, T.; Győrffy, W.; Celani, P.; Werner, H.-J. Communication: Extended Multi-State Complete Active Space Second-Order Perturbation Theory: Energy and Nuclear Gradients. *J. Chem. Phys.* **2011**, *135*, No. 081106.
(37) Dunning, T. H., Jr. Gaussian Basis Sets for Use in Correlated Molecular Calculations. I. The Atoms Boron through Neon and Hydrogen. *J. Chem. Phys.* **1989**, *90*, 1007−1023.
(38) Weigend, F. A Fully Direct RI-HF Algorithm: Implementation, Optimised Auxiliary Basis Sets, Demonstration of Accuracy and Efficiency. *Phys. Chem. Chem. Phys.* **2002**, *4*, 4285−4291.
(39) Shiozaki, T. BAGEL: Brilliantly Advanced General Electronic-Structure Library. *WIREs Comput. Mol. Sci.* **2018**, *8*, No. e1331.
(40) BAGEL *Brilliantly Advanced General Electronic-Structure Library*. Http://Www.Nubakery.Org.
(41) Hirata, S.; Head-Gordon, M. Time-Dependent Density Functional Theory within the Tamm−Dancoff Approximation. *Chem. Phys. Lett.* **1999**, *314*, 291−299.
(42) Becke, A. D. Density-functional Thermochemistry. III. The Role of Exact Exchange. *J. Chem. Phys.* **1993**, *98*, 5648−5652.
(43) Yanai, T.; Tew, D. P.; Handy, N. C. A New Hybrid Exchange−Correlation Functional Using the Coulomb-Attenuating Method (CAM-B3LYP). *Chem. Phys. Lett.* **2004**, *393*, 51−57.
(44) Zhao, Y.; Truhlar, D. G. The M06 Suite of Density Functionals for Main Group Thermochemistry, Thermochemical Kinetics, Noncovalent Interactions, Excited States, and Transition Elements: Two New Functionals and Systematic Testing of Four M06-class Functionals and 12 Other Functionals. *Theor. Chem. Acc.* **2008**, *119*, 525−525.
(45) Chai, J.-D.; Head-Gordon, M. Systematic Optimization of Long-Range Corrected Hybrid Density Functionals. *J. Chem. Phys.* **2008**, *128*, No. 084106.
(46) Stanton, J. F.; Bartlett, R. J. The Equation of Motion Coupled-cluster Method. A Systematic Biorthogonal Approach to Molecular Excitation Energies, Transition Probabilities, and Excited State Properties. *J. Chem. Phys.* **1993**, *98*, 7029−7039.
(47) Wormit, M.; Rehn, D. R.; Harbach, P. H. P.; Wenzel, J.; Krauter, C. M.; Epifanovsky, E.; Dreuw, A. Investigating Excited Electronic States Using the Algebraic Diagrammatic Construction (ADC) Approach of the Polarisation Propagator. *Mol. Phys.* **2014**, *112*, 774−784.
(48) Harbach, P. H. P.; Wormit, M.; Dreuw, A. The Third-Order Algebraic Diagrammatic Construction Method (ADC(3)) for the Polarization Propagator for Closed-Shell Molecules: Efficient Implementation and Benchmarking. *J. Chem. Phys.* **2014**, *141*, No. 064113.

https://doi.org/10.1021/acs.jpca.1c01685
J. Phys. Chem. A XXXX, XXX, XXX−XXX

(49) Shao, Y.; Gan, Z.; Epifanovsky, E.; Gilbert, A. T. B.; Wormit, M.; Kussmann, J.; Lange, A. W.; Behn, A.; Deng, J.; Feng, X.; et al. Advances in Molecular Quantum Chemistry Contained in the Q-Chem 4 Program Package. *Mol. Phys.* **2015**, *113*, 184−215.
(50) Werner, H.-J.; Knowles, P. J. An Efficient Internally Contracted Multiconfiguration−Reference Configuration Interaction Method. *J. Chem. Phys.* **1988**, *89*, 5803−5814.
(51) Knowles, P. J.; Werner, H.-J. An Efficient Method for the Evaluation of Coupling Coefficients in Configuration Interaction Calculations. *Chem. Phys. Lett.* **1988**, *145*, 514−522.
(52) Knowles, P. J.; Werner, H.-J. Internally Contracted Multi-configuration-Reference Configuration Interaction Calculations for Excited States. *Theor. Chim. Acta* **1992**, *84*, 95−103.
(53) Werner, H.-J.; Knowles, P. J.; Knizia, G.; Manby, F. R.; Schütz, M. Molpro: A General-Purpose Quantum Chemistry Program Package. *WIREs Comput. Mol. Sci.* **2012**, *2*, 242−253.
(54) Mozhayskiy, V. A.; Krylov, A. I. *EzSpectrum* Http://Iopenshell.Usc.Edu/Downloads.
(55) *This Work Was Conducted Using the Resources from IOpenShell Center for Computational Studies of Electronic Structure and Spectroscopy of Open-Shell and Electronically Excited Species* (Http://Iopenshell.Usc.Edu) Supported by the National Science Foundation.
(56) Hickman, C. G.; Gascooke, J. R.; Lawrance, W. D. The S_1-$S_0(^1B_2$-$^1A_1)$ Transition of Jet-Cooled Toluene: Excitation and Dispersed Fluorescence Spectra, Fluorescence Lifetimes, and Intramolecular Vibrational Energy Redistribution. *J. Chem. Phys.* **1996**, *104*, 4887−4901.
(57) Minejima, C.; Ebata, T.; Mikami, N. C-H Stretching Vibrations of Benzene and Toluene in Their S1 States Observed by Double Resonance Vibrational Spectroscopy in Supersonic Jets. *Phys. Chem. Chem. Phys.* **2002**, *4*, 1537−1541.
(58) Gardner, A. M.; Green, A. M.; Tamé-Reyes, V. M.; Reid, K. L.; Davies, J. A.; Parkes, V. H. K.; Wright, T. G. The 700-1500 cm^{-1} Region of the S_1 ($\tilde{A}^1$ B_2) State of Toluene Studied with Resonance-Enhanced Multiphoton Ionization (REMPI), Zero-Kinetic-Energy (ZEKE) Spectroscopy, and Time-Resolved Slow-Electron Velocity-Map Imaging (Tr-SEVI) Spectroscopy. *J. Chem. Phys.* **2014**, *140*, No. 114308.
(59) Battaglia, S.; Lindh, R. Extended Dynamically Weighted CASPT2: The Best of Two Worlds. *J. Chem. Theory Comput.* **2020**, *16*, 1555−1567.
(60) Burton, C. S.; Noyes, W. A., Jr. Electronic Energy Relaxation in Toluene Vapor. *J. Chem. Phys.* **1968**, *49*, 1705−1714.
(61) Ray, J.; Ramesh, S. G. Conical Intersections Involving the Lowest $^1\pi\sigma^*$ State in Aniline: Role of the NH2 Group. *Chem. Phys.* **2018**, *515*, 77−87.
(62) Talrose, V.; Stern, E. B.; Goncharova, A. A.; Messineva, N. A.; Trusova, N. V.; Efimkina, M. V. UV/Visible Spectra. In *NIST Chemistry WebBook, NIST Standard Reference Database Number 69*; Linstrom, P. J.; Mallard, W. G. Eds.; National Institute of Standards and Technology: Gaithersburg MD, 2018, 20899.
(63) Sobolewski, A. L.; Domcke, W.; Dedonder-Lardeux, C.; Jouvet, C. Excited-State Hydrogen Detachment and Hydrogen Transfer Driven by Repulsive $^1\pi\sigma^*$ States: A New Paradigm for Nonradiative Decay in Aromatic Biomolecules. *Phys. Chem. Chem. Phys.* **2002**, *4*, 1093−1100.

https://doi.org/10.1021/acs.jpca.1c01685
J. Phys. Chem. A XXXX, XXX, XXX−XXX